

Detecting and drilling in critical inclination window in slant wells by means of a two phase liquid-solid CFD model and experimental study

Mohsen Dehvedar¹, Parviz Moarefvand^{2,*}

¹Dept. of Petroleum Engineering, Amirkabir University of Technology, Iran.

²Dept. of Mining and Metallurgical Engineering, Faculty of Mining, Amirkabir University of Technology, Iran.

* Corresponding author : pmoarefvand@gmail.com

Abstract

Build and hold from vertical section form slant wells. The hole cleaning phenomena in these wells can cause many problems that increase the operational costs. CFD simulation and experimental flow loops are excellent way to study the effect of operational parameters on cutting transport across the annulus. In this study, a liquid-solid CFD model was built that attempted to verify experimental data. The effect of cutting size, drill pipe rotation speed, flow rate, drilling fluid type, and rate of penetration are discussed. The results indicated that there is a specific critical inclination window for slant wells, through with a driller must avoid drilling. Inclinations between 30 to 55° form this window. If there is no way to drill in this range, the operator must increase the flow rate as much as possible and reduce the size of the cuttings in different ways. Increasing the drilling fluid viscosity can also improve hole-cleaning efficiency.

Keywords: CFD; cutting transport; liquid-solid; flow loop; critical inclination window; slant wells

1. Introduction

Since drilling operations are cost-based, cutting transport and hole cleaning are a concern for petroleum engineers (Manjulia *et al.*, 2017). A poor bottom hole cleaning may cause problems. These include an inability to touch the true depth for running casing or liner, lost circulation, excessive torque and drag for pulling the drill string on trips, decreasing the rate of penetration, pipe sticking and excessive bit wearing (Malekzadeh *et al.*, 2011; Cayeux *et al.*, 2016; Han *et al.*, 2016; Ayeni *et al.*, 2016). Computational fluid dynamics (CFD) as a tool for quantitative and qualitative prediction is a good method for studying the main drilling parameter effects on bottom hole cleaning (Moraveji *et al.*, 2017; Heydari *et al.*, 2017; Mohammadzadeh *et al.*, 2016). Studying effective parameters dealing with the subject of hole cleaning on the rig is almost impossible. Therefore, researchers have tried to study them with different flow loops and CFD simulators (Amanna *et al.*, 2016; Kamyab *et al.*, 2016). Many parameters are important for a good hole cleaning. Well designing, wellbore stability, drill string designing, rig capability, mud selection, ECD planning and directional drilling strategies are important concept that need to be addressed. In practice, by focusing on the following parameters, a good hole cleaning includes bottom hole assembly (BHA) design, drill pipe rotation (RPM), flow rate, rate of penetration (ROP), mud weight, mud rheology, down hole drilling dynamics tools, cleanup cycles, and inclination (SEPCO). The

flow loops sketches are based on operational purposes (Falcon, 2009). The main parameters that are studied in the flow loops are inclination, flow rate, cutting and fluid properties, string rotation speed, rate of penetration, and time effects (Egenti, 2014; Nazari *et al.*, 2010). Increases in temperature should also be considered (Wahab *et al.*, 2016). Cutting transport phenomena can be investigated as a liquid-solid system in CFD modeling (Han *et al.*, 2010). In some studies, simulation results were validated against experimental results of flow loops (Kamyab *et al.*, 2016, Sayindla *et al.*, 2017).

Directional wells can be categorized into four types: S-shape, slant, inclined, and horizontal (Figure 1). The slant wells are often called a build and hold. They are drilled vertically from the surface to the kick off point (KOP) at a relatively shallow depth. At that point, the well is steadily and smoothly deflected until a maximum angle and the desired direction are achieved. The established angle and direction are maintained while drilling to the target depth. This method is employed for drilling shallow wells with single producing zones.

In S shape wells, the angle and direction are maintained until a specified depth, then the angle is steadily and smoothly dropped until the well is near vertical and continues into the vertical hole. Inclined wells are a continues build to target. The well is deflected at the KOP, and the inclination is continually built through the target interval. The last well type is horizontal. These wells will have an inclination greater than 80° (Carden *et al.*, 2007).

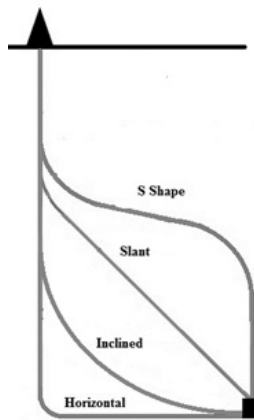


Fig. 1. Different directional wells

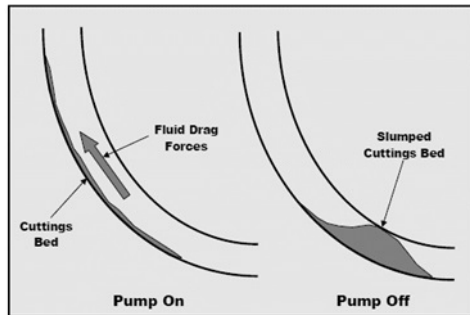


Fig. 2. Cutting bed slumping when pump turned off (Carden *et. al.*, 2007)

In this study, the effect of drilling operation in critical inclinations of slant well types was studied by means of experimental tests and liquid solid computational fluid dynamic simulation. Four nozzles on a drill pipe simulated drill bit nozzles. Other than the annulus, there is an inlet that simulated the formation fluid entrance. In all simulations, the hole cleaning phenomena started when the wait on bit was released. If the pumps turned off during the operation in build sections and also in hold section of slant wells, the cuttings slumped on the low side of the bore hole bottom (Figure 2). In this study, these cuttings were simulated and removed with the help of flow rate, drill pipe rotation speed, and cutting properties. Cutting-size ranges in the CFD model were 1 and 5 mm. In experiments, they were 0.2 and 0.9. The flow rate amounts in the CFD model were 48 and 16 gallons per minute, while in experiments, they were 25 gallons per minute. The critical inclination in the CFD was 30° , while the experimental one was 55° . The drill pipe rotation speeds were 0 and 110 rpm in both the CFD model and experiment.

2. Materials and methods

2.1 Background

Flow loop is predominant method by which petroleum

engineers study the main effective parameters (Allahvirdizadeh *et al*, 2016; Amanna *et al*, 2016; Kamyab *et al*, 2016). The key factor in flow loops is operational pressure. One half of the similar world devices have this limitation. They are divided into two groups, low pressure and high pressure ones. Polyvinyl chloride (PVC) is the material for annulus for low pressure ones, while carbon stainless steel used in high pressure ones. Other constraints are the inclination range, the annulus lengths and diameters (Falcone, 2009). The cutting concentration, bed height and bed length in the annulus, and the volumetric percentage of the cuttings in the outlet are the specific results used as hole cleaning indices (Allahvirdizadeh *et al*, 2016; Tripathy *et al*, 2017). Particle image velocimetry or PIV techniques (Mohammadzadeh *et al*, 2016; Sutkar *et al*, 2013), tomography and gamma ray devices (Limtrakul *et al*, 2005) are recent technologies used for hole cleaning specifications. In this paper, the Amirkabir University flow loop (AUT-PET 01) (Figure 3). The properties of annuli, drilling fluid, cuttings, the drill string, and temperature and pressure can be changed.

2.2 Experimental test setup

For this experiment, the inner pipe was connected with a shaft to the electromotor, the speed of which was controlled by an inverter. The cuttings were injected into the annulus by an electromotor and gearbox system with different rates with a special inlet. The entrance of formation fluid into the annulus was simulated with this input. The inclination was controlled by two arms that were fixed manually from a vertical to horizontal situation. Another input was through the drill string and then from nozzles from which the drilling fluid was injected by a centrifugal pump at different flow rates. The screen was exactly above the drilling fluid tank. After segregation, it moved downward to this tank. A powerful mixer was used to properly mix the drilling fluid. The pressure drop was measured by a Differential Pressure (DP) device, and the data was saved on a PC hard drive by the "Lutron," or a data gathering software.

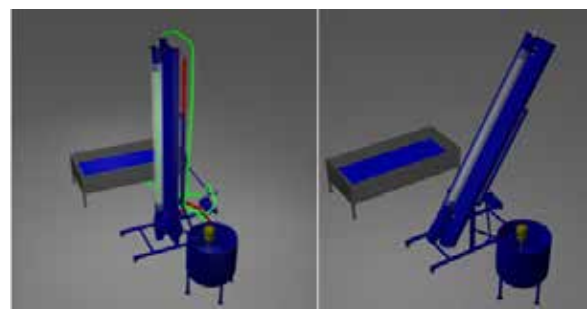


Fig. 3. AUT-PET 01

2.3 Experimental formulation

Skalle's (2010) formula was used for lifting:

$$v_x = \left\{ \frac{4 \left[3\tau_y \left(\phi + \left(\frac{\pi}{2} - \phi \right) \sin^2 \phi - \cos \phi \sin \phi \right) \tan \phi + d_p (\rho_p - \rho) * (\cos \alpha + \sin \alpha \tan \phi) \right]}{3\rho(C_{Drag} + C_{Lift} \tan \phi)} \right\}^{0.5}$$

where v_x (m/s) is the needed velocity for lifting the cuttings across the annulus. The α (degrees) is inclination, and ϕ (degrees) is the repose angle. τ_y is the yield strength of drilling fluid, C_{Lift} is the lift coefficient, and C_{Drag} is the drag coefficient. Finally, ρ_p is the particle or sand density, and ρ is the drilling fluid density.

For the needed velocity of rolling, the following formula (Skalle, 2010) is used:

$$v_x = \left\{ \frac{4 \left[3\tau_y \left(\phi + \left(\frac{\pi}{2} - \phi \right) \sin^2 \phi - \cos \phi \sin \phi \right) + d_p (\rho_p - \rho) \sin \alpha \right]}{3\rho(C_{Drag} - C_{Lift} \tan \phi)} \right\}^{0.5}$$

Gambit software was used to design the main sketch. As shown in Figures 4 and 5, there are 4 nozzles in the drill pipe near the cutting and drilled formation fluid inlet. There is one outlet at the right of the figure.



Fig. 4. The annulus sketch



Fig. 5. 4 nozzles near the inlet

Five mesh types were selected. The properties can be found in Table 1, while their designs are shown in Figure 6.

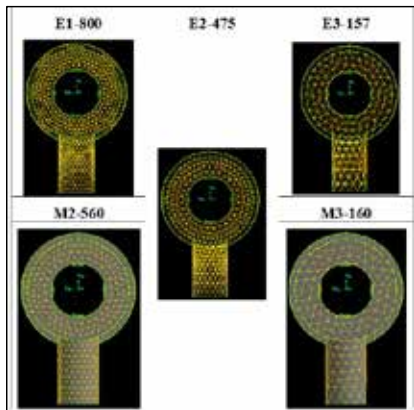


Fig. 6. Different mesh types

Fig. 6. Different mesh types

Mesh name	E1-800	E2-475	E3-157	M3-160	M2-560
Aspect ratio	15.9	15.	25.	25.9	14.5
	9	24	95	5	3
Max ortho skew	0.75	0.7	0.8	0.83	0.72
Min ortho quality	0.18	0.2	0.6	0.64	0.22
Boundary layer	YE	YE	YE	NO	NO
Iteration number	48,000	32,000	28,000	203,000	25,000
Mesh grid * 100000	800	475	157	160	560

2.5 CFD model generation

The solver was pressure-based for absolute velocity formulation in transient flow. The Eulerian-Eulerian model was selected. There were two Eulerian phases. For the viscous model, standard k -epsilon was selected with a standard wall function. Sand and water are the model materials. The granular one was activated for cuttings (See Table 2 for cutting properties).

Table 2. The cutting properties in the model

Sand diameter (m)	0.0009
Granular viscosity (kg/m-s)	Gidaspow
Granular temperature (m ² /s ²)	Algebraic
Solid pressure (Pascal)	Lun et al
Radial distribution	Lun et al
Elasticity modulus (Pascal)	Derived
Packing limit	0.63
Drag	Schiller-Neumann
Restitution coefficient	0.9
Surface tension coefficients (n/m)	0.05

The cutting inlet had a mass flow of 0.3333 kg/s for water as a formation fluid entrance. The nozzles were a velocity inlet with a velocity magnitude of 5.4 m/s that was normal to boundary for water with a 0.008 turbulent viscosity ratio and a 4% turbulent intensity. The outlet was a pressure outlet with 0.001 m²/s² for back flow granular temperature and 0.01 for back flow volume fraction for

Table 3. Model parameters for solution

Pressure-velocity coupling	SIMPLE
Gradient	Least squares cell based
Pressure	PRESTO
Momentum	First order upwind
Volume fraction	QUICK
Turbulent kinetic energy	QUICK
Turbulent dissipation rate	Second order upwind
Energy	First order upwind
Transient formulation	First order implicit

Table 4. CFD Formulation

$\frac{1}{\rho_{Tq}} \left(\frac{\partial}{\partial t} (\alpha_q \rho_q) + \nabla \cdot (\alpha_q \rho_q \vec{V}_q) \right) = \sum_{p=1}^n (m_{pq} - m_{qp})$	Continuity
$\sum \alpha_q = 1$	Summation of volume fractions
$\frac{\partial}{\partial t} (\alpha_s \rho_s \vec{V}_s) + \nabla \cdot (\alpha_s \rho_s \vec{V}_s \vec{V}_s) = -\alpha_s \nabla p - \nabla p_s + \nabla \cdot \vec{\tau}_s + \alpha_s \rho_s \vec{g} + \sum_{i=1}^n [K_{is} (\vec{V}_i - \vec{V}_s) + m_{is} \vec{V}_i - m_{si} \vec{V}_s] + (\vec{F}_s + \vec{F}_{s/f,s} + \vec{F}_{m,s})$	Momentum
$\vec{\tau}_s = \alpha_s \mu_s (\nabla \vec{V}_s + \nabla \vec{V}_s^T) + \alpha_s \left(\lambda_s - \frac{2}{3} \mu_s \right) (\nabla \cdot \vec{V}_s) \vec{I}$	Stress-strain tensor
$K_{si} = \frac{\alpha_s \rho_s f}{\tau_s}$	Solid-liquid diffusion coefficient
$f = \frac{C_D R C_p \alpha_s}{24 W_s^2}$	Friction coefficient
$\tau_s = \frac{\rho_s d_s^2}{18 \mu_s}$	Relaxation time
$K_{is} = \frac{3(1 + \epsilon_{is}) \left(\frac{\pi}{2} + C_{F,1s} \frac{\pi^2}{8} \right) \alpha_s \rho_s \alpha_i \rho_i (d_i + d_s)^2 g_{o,si}}{2\pi (\rho_i d_i^2 + \rho_s d_s^2)} \vec{V}_i - \vec{V}_s $	Interphase exchange coefficient
$\vec{F}_{s/f,s} = -C_L \rho_q \alpha_q (\vec{V}_q - \vec{V}_s) \times (\nabla \cdot \vec{V}_s)$	Lift force
$\theta_s = \frac{1}{3} m_{s,i} m_{s,j}$	Granular temperature
$\frac{3}{2} \left[\frac{\partial}{\partial t} (\rho_s \alpha_s \theta_s) + \nabla \cdot (\rho_s \alpha_s \theta_s \vec{V}_s) \right] = (-\rho_s \vec{I} + \vec{\tau}_s) : \nabla \vec{V}_s + \nabla \cdot (K_{\theta_s} \nabla \theta_s) - \gamma_{\theta_s} + \varphi_{\theta_s}$	The transport equation derived from kinetic theory
$\vec{\tau}_i = \epsilon_i \mu_i (\nabla \vec{u}_i + \nabla \vec{u}_i^T) - \frac{2}{3} \epsilon_i \mu_i (\nabla \cdot \vec{u}_i) \vec{I}$	Liquid stress-strain tensor
$\vec{\tau}_s = \epsilon_s \mu_s (\nabla \vec{u}_s + \nabla \vec{u}_s^T) + \epsilon_s \left(\lambda_s - \frac{2}{3} \mu_s \right) (\nabla \cdot \vec{u}_s) \vec{I}$	Solid stress-strain tensor
$P_s = \alpha_s \rho_s \theta_s + 2\rho_s (1 + \epsilon_{ss}) \alpha_s^2 \theta_{s,ss} \theta_s$	Solid pressure
$\mu_{s,fr} = \mu_{s,cool} + \mu_{s,kin} + \mu_{s,fr}$	Solid shear viscosity
$\mu_{s,cool} = \frac{4}{5} \alpha_s \rho_s d_s g_{o,ss} (1 + \epsilon_{ss}) \left(\frac{\theta_s}{\pi} \right)^{\frac{1}{2}} \alpha_s$	Collisional viscosity
$\mu_{s,fr} = \frac{p_s \sin \phi}{2\sqrt{1-\sin \phi}}$	Frictional viscosity
$\mu_{friction} = \frac{p_{friction} \sin \phi}{2\sqrt{1-\sin \phi}}$	Friction viscosity
$p_{friction} = F_r \frac{(\alpha_s - \alpha_{s,min})^n}{(\alpha_{s,max} - \alpha_s)^n}$	The Johnson and Jackson model for frictional pressure
$\mu_{friction} = p_{friction} \sin \phi$	Frictional viscosity
$\lambda_s = \frac{4}{3} \alpha_s^2 \rho_s d_s g_{o,ss} (1 + \epsilon_{ss}) \left(\frac{\theta_s}{\pi} \right)^{\frac{1}{2}}$	Granular bulk viscosity

$g_{\theta_s} = \left[1 - \left(\frac{\alpha_s}{\alpha_{s,max}} \right)^{\frac{1}{2}} \right]^{-1}$	Radial distribution function
$\gamma_{\theta_s} = \frac{12(1 - \epsilon_{ss}^2) g_{o,ss} \rho_s \alpha_s^2 \theta_s^{\frac{3}{2}}}{d_s \sqrt{\pi}}$	Collisional dissipation of energy
$\vec{\tau}_s = -\frac{\pi}{6} \sqrt{3} \theta_s \frac{\alpha_s}{\alpha_{s,max}} \rho_s g_{o,ss} \sqrt{\theta_s} \vec{u}_{s,i}$	Shear force at the wall
$q_{\theta_s} = \frac{\pi}{6} \sqrt{3} \theta_s \frac{\alpha_s}{\alpha_{s,max}} \rho_s g_{o,ss} \sqrt{\theta_s} \vec{u}_{s,i} - \frac{\pi}{4} \sqrt{3} \frac{\alpha_s}{\alpha_{s,max}} (1 - \epsilon_{ss}^2) \rho_s \theta_s \theta_s^{\frac{3}{2}}$	Granular temperature at the wall

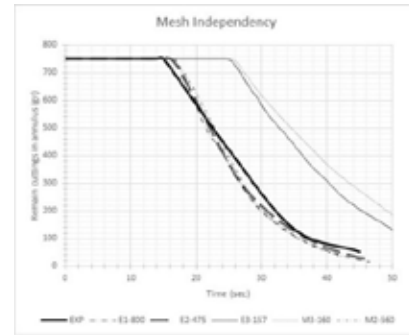
sand the other faces were interiors or walls. The model is solved by the assumptions that are mentioned in Table 3.

The hybrid initialization was carried out, and then the solid phase was patched. The Eulerian multiphase model requires more discussion. The following equations in Table 4 are the most important concepts for the kinetic theory for granular flows.

2.6 Mesh independency

After building the models with different mesh types, the results were compared with the experimental data. The optimum mesh type was selected based on parameters such as time, iteration number, and mesh cell number. The most important factor was the proximity to real data. Figure 7 indicates that E2-475 is the best candidate for this purpose.

The drilling fluid was water like well number 436

**Fig. 7.** Mesh independency

in the Maroon Field of Iran. In addition, pore fluid considered water to have a two-phase liquid solid flow through the annulus. The water injection rate was 5 gallons per minute in the CFD and experimental models, all of which improved the removal of the cuttings.

After detecting the critical inclination in the experiment (tests 1-5) and CFD (tests 6-11), the effect of cutting size (test 12), drill pipe rotation speed (test 13), viscosifier (test 14), cutting type (test 15), cutting type (test 16), and foam (test 17) were analyzed. The effect of the cutting size (test 18), drill pipe rotation speed (test 19) and flow rate (test 20) were investigated in the CFD studies (Table 5).

3. Results and discussion

The worst inclination in the experimental tests was 55°. Here the flow rate was 25 gpm, and the cutting size was 0.9 mm (Figure 8).

In the CFD simulation, the worst inclination could

Table 5. CFD and experimental tests

Test no.	Test name	Inclination (Degrees)	Drill pipe rotation speed (RPM)	Cutting size (mm)	Water flow rate (gpm)	Cutting weight
1	EXP-INC-0	0	110	0.9	25	500
2	EXP-INC-25	25	110	0.9	25	500
3	EXP-INC-45	45	110	0.9	25	500
4	EXP-INC-55	55	110	0.9	25	500
5	EXP-INC-75	75	110	0.9	25	500
6	CFD-INC-0	0	110	1.0	48	750
7	CFD-INC-15	15	110	1.0	48	750
8	CFD-INC-30	30	110	1.0	48	750
9	CFD-INC-45	45	110	1.0	48	750
10	CFD-INC-60	60	110	1.0	48	750
11	CFD-INC-75	75	110	1.0	48	750
12	EXP-CS-55	55	110	1.8	25	500
13	EXP-RPM-55	55	0	0.2	25	500
14	EXP-DFVIS-55	55	110	0.9	25	500
15	EXP-CW-55	55	110	0.9	25	1000
16	EXP-CT-55	55	110	0.2	25	500
17	EXP-DFFOAM-55	55	110	0.9	10	1000
18	CFD-CS-30	30	110	5.0	48	750
19	CFD-RPM-30	30	0	1.0	48	750
20	CFD-FR-30	30	110	1.0	16	750

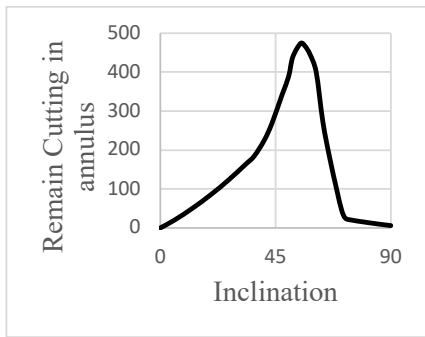


Fig. 8. Experimental critical inclination

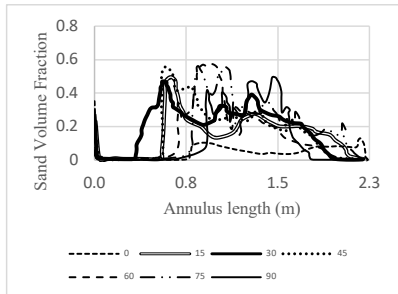


Fig. 9. Volume fraction after 5 seconds

the sand volume fraction after 5 seconds, and Figure 10 shows the sand volume fraction after 10 seconds.

As shown in Figure 10, the cutting bed moved toward the outlet. The 15° had the lowest movement followed by the 30° inclination. The mean bed height in 15° was lower than 30° after 10 seconds but after 5 seconds, the 30° angle had the worst result for bed movement across the annulus. Comparing the figures above, based on sand volume fraction, the critical inclination was 30° in the CFD simulations.

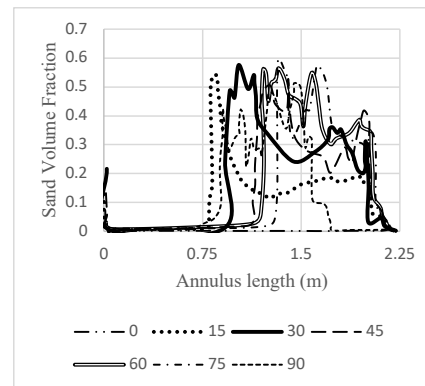
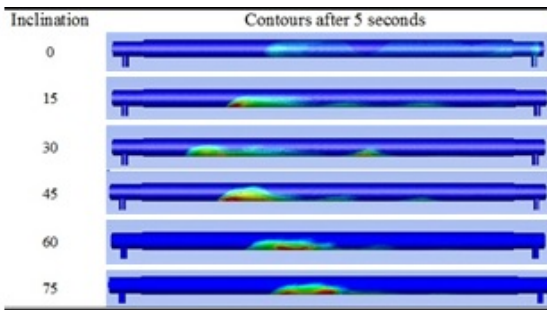


Fig. 10. Sand volume fraction after 10 seconds at different inclinations

gain in different ways. The first method was obtaining by volume fraction at different times. Figure 9 shows

The second way for detecting the critical inclination in CFD modeling is by studying contours. Table 6 shows contours after 5 seconds:

Table 6. Sand contours across the annulus



The above contours show there was a peak in water velocity at the same time as a sand bed peak across the annulus. This is because the cross section area was reduced, and then the water velocity increased. The inclination of 30° had the largest peak across the annulus with the removal of peaks for nozzles and outlet.

As shown in Table 6, the critical inclination was 30. This result confirms that the sand volume fraction result was true. The third way to detect the critical inclination was by comparing the sand velocity and water velocity across the annulus at different times. Figures 11 and 12 can be used to compare the velocities at the 10-second mark.

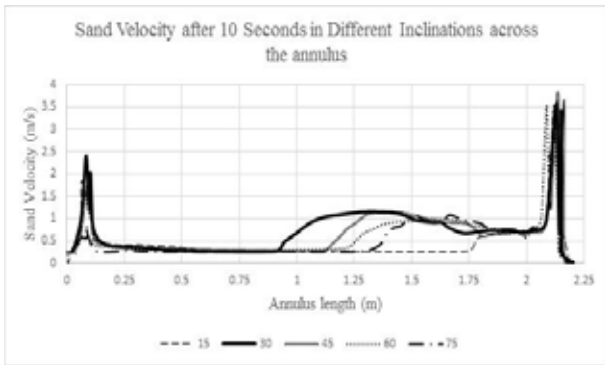


Fig. 11. Sand velocity after 10 seconds in different inclinations across the annulus

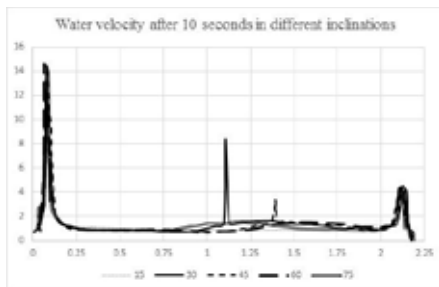


Fig. 12. Water velocity after 10 seconds in different inclinations across the annulus

The final way that was used to detect the critical inclination was to draw the remain cuttings in the annulus at particular time intervals. Figure 13 shows this method.

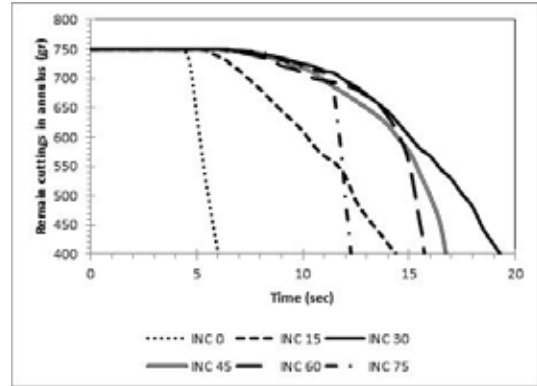


Fig. 13. The remain cuttings in annulus at various times

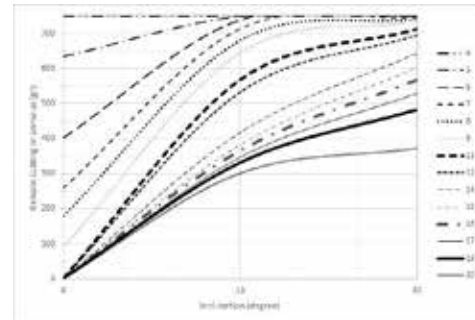


Fig. 14. The remain cuttings in the annulus in 0° to 30° at various times

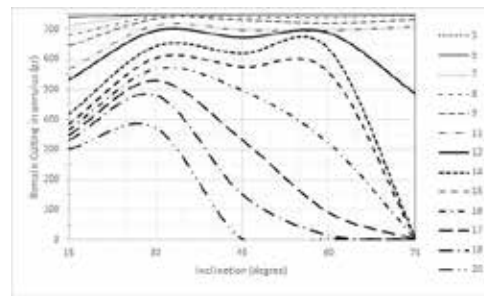


Fig. 15. The remain cuttings in the annulus in 15° to 75° degrees at various times

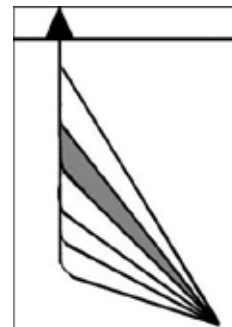


Fig. 16. The critical inclination window for slant wells

The difference between 30° and 15° can be seen in Fig. 13. Figs. 14 and 15 are variations of the data in Figure 13 that help to show the inclination for slant wells at particular timings.

The remain cuttings in the annulus increased from 0° to 30° and then decreased from 30° to 75° during the mention time intervals.

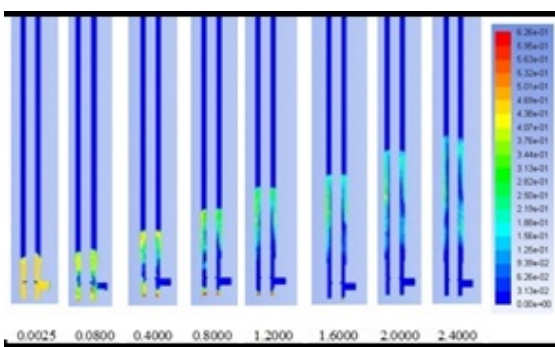
It can be concluded that the critical inclination window was between 30° to 55° based on operational parameters. The red region in Figure 16 shows the critical inclination window.

The above results illustrate that the critical inclination may change under different operational conditions. A well designer must know that operational parameters in the field form a critical inclination window. The hold section in slant wells must be as far as possible from this window.

After detecting the critical inclination, a driller will need to know outcomes if drilling is necessary. For this purpose, the effect of cutting properties, drill pipe rotation speed, and flow rate were considered in the experimental tests and CFD simulations.

In slant wells, there are two main sections: vertical and directional. By increasing the flow rate, hole cleaning efficiency improved in both sections. In addition, by studying the volume fraction of cuttings through the annulus in the vertical sections, almost no cutting remained, unless a small amount fell to the bottom of the setup. Table 7 shows the volume fraction of the upward cuttings at plane $z=0$ at different time intervals.

Table 7. Volume fraction of upward cuttings at plane $z=0$ and the whole annuli



The sand velocity after 5 and 10 seconds in the vertical section is shown in Figure 17. The velocity is high near the inlet area and nozzles and is low near the outlet. The sand velocity diagram after 10 seconds shows that the bed moves during the time. This velocity is related to the sands that are in above the bed and the water velocity move them along the annulus

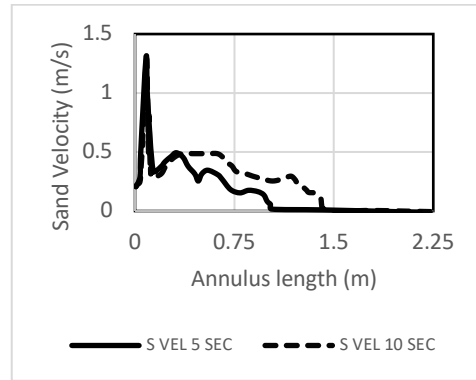


Fig. 17. Sand velocity after 5 and 10 seconds in vertical section

Using viscosifiers improved hole cleaning at critical inclination. The Figure 18 shows the rheological properties of the EXP-DFVIS-55 fluid. Using foam as a drilling fluid had a very good effect on cutting transport, especially in the vertical section. It is recommended for use whenever possible. In slant wells, it is particularly recommended because the bed height is reduced and then the sticking possibility is decreased (Figure 18)

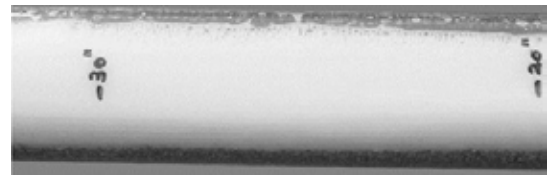


Fig. 18. Using foam as drilling fluid

Reducing the size of the cuttings from 0.9 mm to 0.2 mm in the experiments, and also removing the pipe rotation speed in critical inclination caused an interesting experimental outcome. Reducing the cutting size transforms the cutting beds into moving hills. In addition, removing the drill string rotation will make the cuttings moving hills joint with each other. But in some solids-liquid flow in pipe, there is no pipe rotation and solid moving hills are also observed (Figure 19). Because of these outcomes, the relationships between cutting bed shape, cutting size, and pipe rotation should be investigated more deeply.



Fig. 19. The effect of pipe rotation on hole cleaning (size 0.2 mm)

Increasing the size of the cuttings in the experiment from 0.9 to 1.8 mm and in the CFD model from 1 to 5 mm increased the amount of them through the annulus. In other words, operational problems increase. Increasing the amount of the cuttings can be related to an increase in the rate of penetration (ROP). In this situation, the amount of cuttings, the bed length, and height increase. Hole cleaning problems, such as sticking, also increased. Increasing the wait on bit (WOB), can increase the rate of penetration (ROP) until critical points (Figure 20, point d). The amount of cuttings went up. By increasing the amount of injected cuttings, it may cause a mistake that the hole cleaning efficiency is improved but it's not forgotten that this work can lead to a stuck.

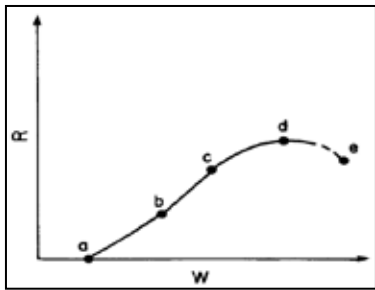


Fig. 20. The effect of wait on bit (W) on the penetration rate (R) (Bourgoyne *et al*, 1991)

As shown in Figure 20, the WOB must reach to specific point (a) until penetration has been started. After this point, a rapid increase can be seen (ab). At an intermediate WOB, a linear increase is evident (bc). At a higher WOB, the ROP slightly increased (cd). After a specific amount of WOB, by increasing it, the ROP decreased (de). As discussed, the weak response to the higher WOB loads usually to the lower HCI (Bourgoyne *et al*, 1991). Figure 21 shows the relation between the ROP and drill pipe rotation at the conditions at which the other parameters are fixed.

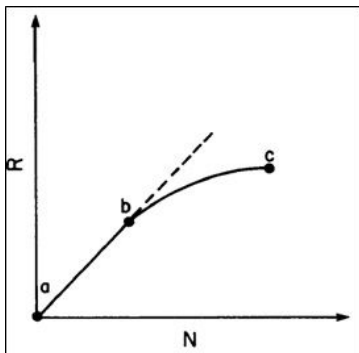


Fig. 21. The effect of drill pipe rotation (N) on the rate of penetration (R) (Bourgoyne *et al*, 1991)

At lower rates of penetrations, and by increasing drill pipe rotation speed, the ROP increased linearly and at a higher rate of penetration. When it was raised, the ROP rate decreased and lead to low hole cleaning efficiency. It must be considered that in high flow rates removing the drill pipe rotation has no effect on hole cleaning of slant wells.

Decreasing the flow rate from 48 to 16 gallons per minute increased the cuttings concentration amount in the annulus. The brief results of changing the effective parameters is shown in Figure 22.

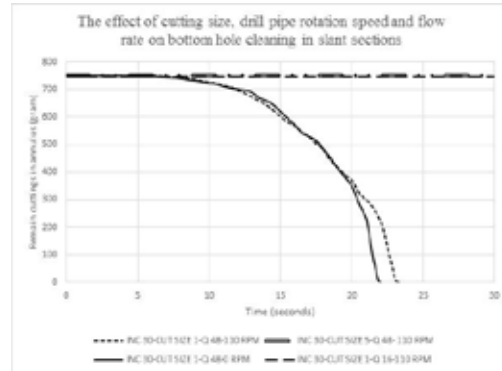


Fig. 22. The brief results of changing the operational parameters

As shown in Figure 22, removing the drill pipe rotation speed enhanced the hole cleaning in high flow rates. Increasing the size of the cuttings from 1 to 5 mm and decreasing the flow rate from 45 to 16 gpm almost have a similar effect on hole cleaning of slant sections.

4. Conclusion

The following conclusions on critical inclination of slant wells can be drawn from this research:

1. There is a critical inclination window based on the main parameter range.
2. Well designers must avoid the critical inclination window when designing well trajectory.
3. The critical inclination for cutting transport can be determined with using water velocity and sand volume fraction contours.
4. Reducing the cutting size from 0.9 to 0.2 mm will change a cutting bed into moving hills, and removing drill pipe rotation will make these hills joint together.
5. Increasing the cutting size from 1 to 5 mm and decreasing the flow rate from 48 to 16 gpm increase the amount of the cuttings in the annulus. There was virtually no cutting in the annulus outlet.
6. Increasing the flow rate can compensate for defects from other parameters, such as increasing the cutting size on hole cleaning phenomena.
7. Viscosifier materials and foams can improve

drilling fluid ability and is better than water for removing the cuttings in the critical inclination of slant wells.

8. A weak response to the higher WOB loads usually leads to a lower hole cleaning efficiency.

9. At lower rates of penetration, with increasing it, the ROP increased linearly and at a higher rate of penetration, with increasing it, The ROP rate decreased and led to inefficient hole cleaning.

5. Nomenclature

q_s	Granular temperature at the wall
p_s	Solid Pressure
$K_{\theta s}$	Diffusion coefficient for granular energy
$\alpha_{s,max}$	Maximum packing limit
g_o	Radial distribution function
$\mu_{s,fr}$	Friction viscosity
$\mu_{s,kin}$	Kinetic viscosity
$\mu_{s,col}$	Collisional viscosity
λ_q	Bulk viscosity
K_{ls}	Interphase exchange coefficient
f	Friction coefficient
$\overline{\tau}_q$	Stress-strain tensor
$F_{net,rolling}$	Net force for rolling the particle (N)
ϕ	Repose angle (degrees)
C_{drag}	Drag coefficient
v_x	Velocity (m/s)
μ_s	Solid shear viscosity
θ_s	Granular temperature
Φ_{ls}	Energy exchange between phases
γ_{θ_s}	Collisional dissipation of energy
τ_s	Relaxation time
α	Volume fraction
e_{ls}	Coefficient of restitution
$g_{o,ls}$	Radial distribution coefficient
d_p	Particle diameter (m)
Re_p	Particle Reynolds number
τ	Shear stress (Pascal)
τ_y	Yield strength of drilling fluid (Pascal)
$F_{net,lift}$	Net force for lifting the particle (N)
α	Inclination (degrees)
C_{lift}	Lift coefficient
ρ	Density (kg/m ³)

References

Allahviridizadeh, P., Kuru, E. & Parlaktuna, M. (2016). Experimental investigation of solids transport in horizontal concentric annuli using water and drag reducing polymer-based fluids. *Journal of Natural Gas Science and Engineering*, **35**: 1070-1078.

Amanna, B. & Movaghar, M.R.K. (2016). Cuttings transport behavior in directional drilling using computational fluid dynamics (CFD). *Journal of Natural Gas Science and Engineering*, **34**: 670-679.

Ayeni, O.O., Wu, C.L., Nandakumar, K. & Joshi, J.B. (2016). Development and validation of a new drag law using mechanical energy balance approach for DEM–CFD simulation of gas–solid fluidized bed. *Chemical Engineering Journal*, **302**: 395-405.

Bourgoyne, A.T., Millheim, K.K., Chenevert, M. E. & Young, F.S. (1991). *Applied drilling engineering*, Vol. 2. Richardson, TX: Society of Petroleum Engineers. pp. 137-144

Carden, R.S. & Grace, R.D. (2007). *Horizontal and directional drilling*. Tulsa, Oklahoma: Petroskills, LLC.

Cayeux, E., Leulseged, A., Kluge, R. & Haga, J. (2016). Use of a transient cuttings transport model in the planning, monitoring and postanalysis of complex drilling operations in the North Sea. In *IADC/SPE Drilling Conference and Exhibition*. Society of Petroleum Engineers.

Egenti, N.B. (2014). Understanding drill-cuttings transportation in deviated and horizontal wells. Paper presented at the SPE-172835-MS, Lagos, Nigeria.

Falcone, G. (2009). Flow loops for validating and testing multiphase flow meters. *Developments in Petroleum Science*, **54**: 295-302.

Han, S.M., Hwang, Y.K., Woo, N.S. & Kim, Y.J. (2010). Solid–liquid hydrodynamics in a slim hole drilling annulus. *Journal of Petroleum Science and Engineering*, **70**(3): 308-319.

Han, S.M., Woo, N.S. & Kim, Y.J. (2016). A study of the particle transport in the non-newtonian fluid with inclined annulus. *Asia-Pacific Journal of Modeling and Simulation for Mechanical System Design and Analysis*, **1**(1): 23-28.

Heydari, O., Sahraei, E. & Skalle, P. (2017). Investigating the impact of drill pipe's rotation and eccentricity on cuttings

- transport phenomenon in various horizontal annuluses using computational fluid dynamics (CFD). *Journal of Petroleum Science and Engineering*, **156**: 801-813.
- Kamyab, M. & Rasouli, V. (2016).** Experimental and numerical simulation of cuttings transportation in coiled tubing drilling. *Journal of Natural Gas Science and Engineering*, **29**: 284-302.
- Limtrakul, S., Chen, J., Ramachandran, P.A. & Duduković, M.P. (2005).** Solids motion and holdup profiles in liquid fluidized beds. *Chemical Engineering Science*, **60**(7): 1889-1900.
- Manjula, E.V., Ariyaratne, W.H., Ratnayake, C. & Melaen, M. C. (2017).** A review of CFD modelling studies on pneumatic conveying and challenges in modelling offshore drill cuttings transport. *Powder Technology*, **305**: 782-793.
- Mohammadsalehi, M. & Malekzadeh, N. (2011).** Optimization of hole cleaning and cutting removal in vertical, deviated and horizontal wells. In *SPE Asia-Pacific Oil and Gas Conference and Exhibition*. Society of Petroleum Engineers.
- Mohammadzadeh, K., Hashemabadi, S.H. & Akbari, S. (2016).** CFD simulation of viscosity modifier effect on cutting transport by oil based drilling fluid in wellbore. *Journal of Natural Gas Science and Engineering*, **29**: 355-364.
- Moraveji, M.K., Sabah, M., Shahryari, A. & Ghaffarkhah, A. (2017).** Investigation of drill pipe rotation effect on cutting transport with aerated mud using CFD approach. *Advanced Powder Technology*, **28**(4): 1141-1153.
- Nazari, T., Hareland, G. & Azar, J.J. (2010).** Review of cuttings transport in directional well drilling: Systematic approach. In *SPE Western Regional Meeting*. Society of Petroleum Engineers.
- Sayindla, S., Lund, B., Ytrehus, J.D. & Saasen, A. (2017).** CFD modelling of observed cuttings transport in oil-based and water-based drilling fluids. In *SPE/IADC Drilling Conference and Exhibition*. Society of Petroleum Engineers.
- Skalle, P. (2010).** *Drilling fluid engineering*. London, Bookboon.Pp. 76.
- Sutkar, V.S., Deen, N.G. & Kuipers, J.A. (2013).** Spout fluidized beds: Recent advances in experimental and numerical studies. *Chemical engineering science*, **86**: 124-136.
- Tripathy, A., Bagchi, S., Biswal, S.K. & Meikap, B.C. (2017).** Study of particle hydrodynamics and misplacement in liquid–solid fluidized bed separator. *Chemical Engineering Research and Design*, **117**: 520-532.
- Wahab, H.A., Hussain, S. & Naeem, M. (2016).** Mixed convection flow of Powell-Eyring fluid over a stretching cylinder with Newtonian heating. *Kuwait Journal of Science*, **43**(3): 01-13.

Submitted :17/10/2017

Revised :19/12/2017

Acceptance :20/12/2017

ثنائي الطور (الصلب - CFD) الكشف والحفر في نافذة الميل الحرج في الآبار المائلة بواسطة نموذج ديناميك الموائع الحسابي (الساائل) ودراسة تجريبية

محسن ديهفیدار¹، بارفيز مواريفاند²

¹ قسم هندسة البترول، جامعة أميركابير للتكنولوجيا (طهران البوليتكنك)، طهران، إيران
² قسم هندسة التعدين والفلات، جامعة أميركابير للتكنولوجيا (طهران البوليتكنك)، طهران، إيران

المخلص

إن البناء والتحميل من قطاع عمودي يشكل الآبار المائلة. ويمكن لظاهرة تنظيف الثقوب في هذه الآبار أن تسبب الكثير من المشاكل التي تزيد من تكاليف التشغيل. إن نموذج محاكاة ديناميك الموائع الحسابي (CFD) وحلقات التدفق التجريبية هي أجهزة جيدة لدراسة تأثير المعلمات التشغيلية على نقل كسارة الحفر عبر الحلقة. في هذه الدراسة حاولنا بناء نموذج CFD ساائل - صلب تم التحقق منه باستخدام بيانات تجريبية. تمت مناقشة تأثير حجم الكسارات وسرعة دوران أنبوب الحفر ومعدل الجريان ونوع ساائل الحفر ومعدل الاختراق. وأشارت النتائج إلى وجود نافذة ميل حرجة خاصة بالآبار المائلة ويجب على الحفار تجنب الحفر فيها. تُشكل الميول ما بين 30 إلى 55 درجة هذه النافذة. وإذا لم تكن هناك طريقة للحفر في هذه الزاوية، يجب على المشغل زيادة معدل الجريان قدر الإمكان، وأن يحاول تقليل حجم الكسارات بطرق مختلفة. وقد أدت زيادة لزوجة ساائل الحفر إلى تحسين كفاءة تنظيف الثقب.